Biomicrofluidics ARTICLE scitation.org/journal/bmf

Enhanced blebbing as a marker for metastatic prostate cancer

Cite as: Biomicrofluidics 13, 034110 (2019); doi: 10.1063/1.5085346
Submitted: 11 December 2018 · Accepted: 22 April 2019 ·
Published Online: 21 May 2019

Zeina S. Khan, Julianna M. Santos, Neil G. Vaz, and Fazle Hussain[a)]

AFFILIATIONS

Department of Mechanical Engineering, Texas Tech University, Lubbock, Texas 79409, USA

[a)]**Electronic mail:** fazle.hussain@ttu.edu

ABSTRACT

Highly metastatic prostate cancer cells flowing through a microfluidic channel form plasma membrane blebs: they form 27% more than normal cells and have a lower stiffness (about 50%). Hypo-osmotic stress assays (with ∼50% osmolarity) show 22% more blebbing of highly metastatic than moderately metastatic and 30% more than normal cells. Plasma membrane blebbing is known to provide important metastatic capabilities to cancer cells by aiding cell detachment from the primary tumor site and increasing cell deformability to promote cell migration through the extracellular matrix. Increased blebbing was attributed by others to decreased phosphorylated ezrin, radixin, and moesin (ERM) (p-ERM) protein expression—p-ERMs bind the plasma membrane to the actin cortex and reduced p-ERM expression can weaken membrane-cortex attachment. Myosin II also influences blebbing as myosin's natural contraction generates tension in the actin cortex. This increases cellular hydrostatic pressure, causes cortex rupture, cytoplasm flow out of the cortex, and hence blebbing. Highly metastatic cells are surprisingly found to express similar ezrin and myosin II levels but higher moesin levels in comparison with lowly metastatic or normal cells—suggesting that their levels, contrary to the literature [G. Charras and E. Paluch, Nat. Rev. Mol. Cell Biol. **9**(9), 730–736 (2008); J.-Y. Tinevez, U. Schulze, G. Salbreux, J. Roensch, J.-F. Joanny, and E. Paluch, Proc. Natl. Acad. Sci. U.S.A. **106**(44), 18581–18586 (2009); M. Bergert, S. D. Chandradoss, R. A. Desai, and E. Paluch, Proc. Natl. Acad. Sci. U.S.A. **109**(36), 14434–14439 (2012); E. K. Paluch and E. Raz: Curr. Opin. Cell Biol. **25**(5), 582–590 (2013)], are not important in metastatic prostate cell blebbing. Our results show that reduced F-actin is primarily responsible for increased blebbing in these metastatic cells. Blebbing can thus serve as a simple prognostic marker for the highly incident and lethal metastatic prostate cancer.

I. INTRODUCTION

Protrusion formation is essential for cell migration. *In vivo* and *in vitro* studies have shown that cancer cells migrate by generating lamellipodia driven by actin polymerization (mesenchymal migration) and blebs driven by actomyosin contractions (amoeboid migration).[3] The ability of cancer cells to switch between protrusion types in response to chemotherapy drugs and environmental changes[1,4–6] demonstrates their plasticity and may result in wide metastatic spreading by promoting cell detachment from the primary tumor site and increasing cell deformability aiding travel through the extracellular matrix (ECM).[7,8] Blebbing may therefore be a marker for metastatic cancer. Some studies have shown that increased blebbing is correlated with decreased expression of ERM (ezrin, radixin, and moesin) proteins that link the plasma membrane to the actin cortex—underexpression of these proteins may result in weaker plasma membrane-cortex attachments, which may lead to bleb formation.[9–11] Myosin II has also been shown to contribute to blebbing, as myosin II's innate contractions produce tension in the actin cortex, resulting in increased hydrostatic pressure in the cytoplasm and rupturing the cortex leading to cytoplasm flow and bleb formation.[1–4]

Prostate cancer is the second most incident and is the second-leading cause of male cancer deaths worldwide.[12,13] The American Cancer Society and American Urologic Association recommend annual prostate specific antigen (PSA) screening for all men above 50; however, surprisingly, many highly metastatic prostate cancers lack PSA.[14] Treatment of prostate cancer is also complex as many early-stage and lowly metastatic prostate cancers are androgen sensitive and are well-treated with androgen suppression or ablation therapy. The majority of prostate tumor cells that survive this treatment become androgen insensitive and metastatic.[15] There is currently a need to develop better tools for detecting

metastatic prostate cancer that do not solely rely on PSA[13] and can additionally grade androgen insensitive cells, since metastasis is the primary cause of prostate cancer deaths.

Cancer cells undergo many changes in protein expressions as they become more metastatic; frequently observed reduction in F-actin levels result in changes in cell morphology[16] and cell stiffness[17–22]—where increased deformability (or reduced stiffness) can be used as a marker for many different types of metastatic cancer. This increased deformability may also enable metastatic spread, as the cells can migrate more easily through confining extracellular matrix spaces and form invadopodia—actin-rich protrusions of the plasma membrane involved in degrading the extracellular matrix—more easily.[23]

Previous prostate cancer cell studies, however, have made a differing observation: that cell stiffness does not always decrease with increasing metastatic potential.[13,24] These studies compared the stiffness of lowly metastatic androgen sensitive cells with highly metastatic androgen insensitive cells,[13,24] where it was found that androgen sensitive cells were the least stiff. It is known that androgen sensitive prostate cancer cells translocate cleaved filamin proteins to the nucleus.[25,26] The intact actin cross-linking filamin protein is known to significantly stiffen actin networks;[27,28] therefore, its cleavage (the process of breaking peptide bonds between the amino acids in proteins) and nuclear localization can result in lowly metastatic androgen sensitive cells having a low stiffness in comparison with highly metastatic androgen insensitive cells. Here, we compare the mechanical properties of androgen insensitive highly and moderately metastatic with normal prostate cells, to see if cell stiffness decreases with increasing metastatic potential in deadly androgen insensitive cells. Androgen sensitive cells were not included since previous studies[13,24] have shown that these cells are significantly softer than highly metastatic prostate cancer cells.

We have investigated the suitability of both blebbing and cell stiffness as markers for metastatic androgen insensitive prostate cancer using microfluidic devices to deform cells and perform rheological measurements and hypo-osmotic stress assays to induce bleb formation. Our device—see Sec. II for details, and Fig. 1 and Fig. 1 in the supplementary material for illustrations—is designed to mimic the travel of cells through confined spaces resembling tumor extracellular matrices. Fibrillar extracellular matrix tissues can have gap diameters of less than 5 μm to larger than 20 μm.[29] Our simple and inexpensive device is the first microfluidic device used for measuring both cell blebbability and rheology, and these methods have the potential to be adapted for high-throughput clinical applications.

We used the highly metastatic PC3 cell line, obtained from bone metastasis, which is a widely used model for prostate cancer lacking PSA.[12] The DU145 cell line, obtained from brain metastasis and also lacking PSA,[30] was used as a moderately metastatic model cell line. The RWPE-1 prostate cell line, an established epithelial line created from a white male's tissue donation and immortalized using human papilloma virus 18,[31] was used as a normal cell control. These cancer cell lines have been used in previous cancer cell rheological studies;[13,32] however, the blebabbility, stiffness, and fluidity have not been studied concomitantly. The number of blebbing cells, blebbing frequency, and reduced cell stiffness are found to be good markers for metastatic prostate cancer cells since metastatic cells bleb more frequently and are significantly less stiff than normal cells. We investigated the mechanism for bleb formation using western blots for ezrin, moesin, and myosin II, and fluorescent staining for F-actin, and found that reduced F-actin is primarily related to the increased metastatic cell blebbing, in contrast to the literature.[1–4,9–11]

II. MATERIALS AND METHODS

A. Cell culture

All cells were cultured at 37 °C and 5% CO_2. Prostate cancer (highly metastatic PC3 and moderately metastatic DU145) and normal prostate cells (RWPE-1) were provided by Dr. Stephanie Filleur (Texas Tech University Health Sciences Center, Lubbock, TX). The PC3 and DU145 cell lines are androgen insensitive since they do not express androgen receptors.[35] RWPE-1 cells also do not express androgen receptors.[36] PC3 and DU145 were cultured in RPMI 1640 medium with L-glutamine (Gibco 10-040-CV, Thermo Fisher Scientific, MA), supplemented with 10% fetal bovine serum (FBS) (Gibco 10437-028) and 1% penicillin-streptomycin (Gibco, 15140-122). RWPE-1 cells were grown in Keratinocyte-SFM (1×) serum-free media with L-glutamine (Gibco, 10724-011), Epidermal Growth Factor and Bovine Pituitary Extract (Gibco, 13028-014 and 10450-013), and 1% penicillin-streptomycin.

For every passage and for experiments, cells were harvested by incubating with trypsin [Gibco by Life Technologies, 25302-062—5 ml per flask for cancer cells, 5 ml of a 1:1 trypsin–Dulbecco's phosphate-buffered saline (DPBS) mixture for RWPE-1] at 37 °C—3 min for PC3 and DU145, and 8 min for RWPE-1. Trypsin was inhibited for cancer cells by adding 500 μl FBS. Trypsin was inhibited with DPBS containing 0.1% FBS for RWPE-1. Cells were centrifuged for 5 min at 1000 rpm (Eppendorf Centrifuge 5804R, Hauppauge, NY), the supernatant was removed, cells were suspended in 2–4 ml of fresh medium, and counted with trypan blue (Corning, 25900CI) using an automated cell counter (TC20, Bio-Rad, Berkeley, CA).

B. Microfluidic device design, fabrication, and operation

The microfluidic devices had wide inlet and outlet channels (100 μm wide and 300 μm long) meeting a narrow channel in the center (150 μm long, 8–9 μm wide, and 11 μm high)—see Fig. 1 in the supplementary material. The molds for the devices were made using standard soft lithography techniques with a negative photoresist.[37] Polydimethylsiloxane (PDMS) (Sylgard 184 silicone elastomer kit, Dow Corning) was degassed, poured into the mold, and baked for 2 h at 80 °C. After baking, the PDMS was cut, peeled, and inlet and outlet holes were punched (Harris Uni-core 0.75 mm outer diameter, GE Healthcare Bio-Sciences). Devices were bonded to glass coverslips by exposing them to air plasma (PDC-32G, Harrick Plasma), putting them into contact, and baking the bonded devices at 80 °C for 20 min.

Cells were treated with NucBlue (R37605, Thermo Fisher Scientific) nuclear stain following manufacturer's instructions, trypsinized, centrifuged, and resuspended in a mixture of Trypan blue and medium (2:1) with 0.01% Pluronic F-127 (P2443, Sigma-Aldrich) to

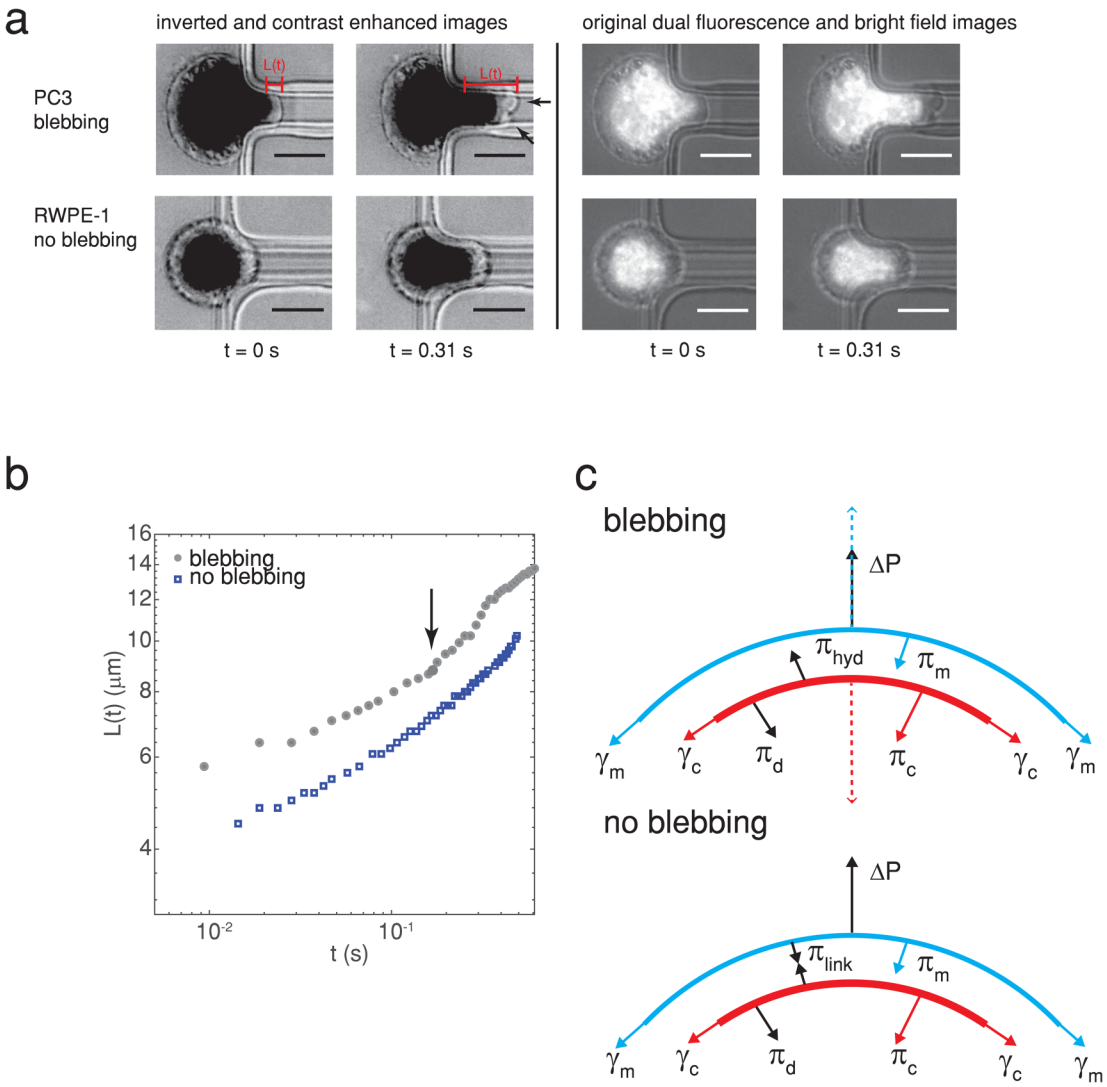

FIG. 1. (a) A highly metastatic PC3 prostate cancer cell forms plasma membrane blebs when flowing into a constricted microfluidic channel (upper panel), while a normal RWPE-1 prostate cell does not (lower panel). Arrowheads indicate blebs. The images on the left are inverted and contrast enhanced (grayscale values in the range of [0 128] were stretched to [0 255]), and nuclei were fluorescently stained with Hoechst 33342. Scale bars represent 10 μm. The original unenhanced dual fluorescence and bright-field images are shown on the right. The pressure drop across the cell is 1000 Pa. The time $t = 0$ when the cell first enters the channel is determined from videography. The cell extension length $L(t)$ is measured from images such as these and used to calculate rheological creep $J(t)$. The power law fits to $J(t)$ vs t give the cells' stiffness and fluidity (see the main text for details). (b) The temporal change in the cell extension length for a blebbing and nonblebbing cell [both from (a)], where an arrow indicates the onset of bleb formation. (c) Simple model of the forces exerted on the plasma membrane, actin cortex, and membrane-cortex linkers for a nonblebbing (no blebbing, bottom) and a blebbing cell (top). The main forces for a nonblebbing cell are the pressure drop across the cell ΔP, the membrane tension γ_m resulting in pressure π_m, the cortical tension γ_c resulting in pressure π_c, the force exerted on the plasma membrane and cortex by linker proteins resulting in pressure π_{link}, and the pressure resulting from viscous dissipation and friction π_d. Arrows indicate the direction that the forces act. For a sufficiently high distribution of linkers and low pressure drop (typically < 1000 Pa[10]), the plasma membrane does not become detached from the actin cortex. When ΔP is sufficiently large to detach the linker proteins, the actin cortex moves inwards toward the center of the cell due to cortical tension as denoted by the dashed red arrow, driving cytoplasmic fluid toward the plasma membrane resulting in a hydrodynamic pressure π_{hyd}. This causes a bleb to form, pushing the plasma membrane outwards as depicted by the blue dashed arrow.[10,33,34]

reduce nonspecific cell adhesion.[38] Trypan blue was used to exclude dead cells from analysis. Cell suspensions were pipetted into MFCS-EZ microfluidic flow controller reservoirs (Fluigent), reservoirs were attached to the flow controller, and the cells were pushed with constant pressure drops ranging from 1000 to 4000 Pa.[39] The outlets were exposed to the atmosphere, giving a pressure drop across the cell equal to the difference in applied and outlet pressures when a cell blocks the narrow channel. Images

were obtained at 40× magnification using phase contrast and DAPI fluorescence modes simultaneously with a Nikon Eclipse microscope (Eclipse Ti, Nikon, NY). Images were recorded with a Zyla 4.2 sCMOS (Andor) at 100–200 fps and 0.16 μm/pixel. All experiments were performed at 37 °C.

C. Cell rheology measurements

To determine the stiffness $1/A$ and fluidity α power law rheology parameters, the cell extension length $L(t)$ in a narrow channel was measured (see Fig. 1). The entry of the channel, defined as the region where the constricted channel entrance was not curved (due to a fillet), was found by drawing straight lines along the narrow channel's sidewalls. $L(t)$ was the distance of the front end of the cell from the channel entrance measured at the center of the channel. The rheological creep $J(t) = (2\pi\phi L(t))/(3R_P\Delta P)$[40] was calculated during cell entry into the channel for small deformations—prior to bleb formation and growth for blebbing cells. R_P is the hydraulic radius of the channel (4–5 μm), the constant ϕ has the value 1.4,[41] and $\Delta P = 1000–2000$ Pa is the pressure drop across the cell while it is entering the channel. Both radius and pressure drop values were similar to our prior cell mechanics study on breast cancer cells treated with Vitamin D_3 and in control conditions;[38] note that this paper's objective and results are totally different from Ref. 38. A and α were obtained from the power law fits to nucleus creep against time $J(t) = (A/\alpha\Gamma(\alpha))(t/t_0)^{\alpha}$. A has units of Pa^{-1} by setting $t_0 = 1$ s, consistent with prior studies.[38,40] Γ is the Gamma function. Data and image analysis were performed with ImageJ and Matlab.

D. Hypo-osmotic stress assay

The response of prostate cells to hypo-osmotic conditions was studied by removing the cell culture media (osmolarity 280–300 mOsm/kg) and replacing the media with a 2:1 mixture of ultrapure Milli-Q water and media (MilliQ Advantage, EMD Millipore, CA). These mixtures had osmolarities in the range of 120–140 mOsm/kg as measured by a VAPRO vapor pressure osmometer (5520, Wescor, UT). After media replacement, cells were imaged in the phase contrast mode with a Nikon Eclipse Ti microscope at 37 °C and 5% CO_2 for 12 h. The number of blebbing cells in the images was counted over the course of 12 h. Control cells were incubated with culture media and imaged under the same conditions as hypo-osmotic cells. Cell counting with trypan blue, described above, was used to quantify the effect of hypo-osmotic treatment on cell viability in comparison with control cells.

E. Fluorescence staining

Cells were plated on coverslips until subconfluent, fixed with 4% paraformaldehyde, quenched with phosphate buffer saline (PBS) and 50 mM NH_4Cl (Sigma-Aldrich, 213330) for 10 min, permeabilized with 0.1% PBS-Triton for 10 min, and blocked with 1% PBS-BSA (Sigma-Aldrich, A2153) for 15 min. Samples were incubated with alexa fluor phalloidin 488 (dilution 1:300 in PBS-BSA, Molecular probes by Life Technologies, A12379) that specifically stains F-actin, for 1 h. After staining, the coverslips were washed 7 times with PBS and mounted on glass slides using Prolong Gold antifade reagent with DAPI nuclear stain (Molecular probes by Life Technologies, P36935). Images were obtained at 90× magnification using a Nikon Eclipse microscope. The corrected cell fluorescence density, taking into account background fluorescence, was calculated as $CCFD = CID - MBI \times Area$, where $CCFD$ is the corrected cell fluorescence density, CID is the integrated cell fluorescence density (the product of average cell grayscale and cell area), MBI is the average background intensity (averaged over 8 regions near the cell), and $Area$ is the cell area.[42] $CCFD$ was calculated from raw fluorescence images.

F. Subcellular fractionation

Prostate cells were trypsinized, washed twice with cold PBS, and resuspended in 3 ml of the lysis buffer (Pierce IP Lysis Buffer, Thermo Fisher Scientific, 87788) supplemented with a protease inhibitor cocktail (Halt protease inhibitor cocktail, Thermo-Fisher Scientific, 87786) at the concentration recommended by the manufacturer. Cells were homogenized 20 times in a teflon/glass dounce homogenizer; this suspension was stored as a homogenate fraction (containing all cellular fractions) at −80 °C. The protein concentration was determined with a spectrophotometer/fluorometer at 280 nm (DeNovix, DS-11 FX+, Wilmington, DE) prior to performing western blots.

G. Western blots

Homogenate fractions (30 μg protein) were diluted 1:1 in the laemmli sample buffer (Bio-Rad, 161-0737) with 50 μl of 2-mercaptoethanol (Bio-Rad, 161-0710), placed in 4%–20% gradient acrylamide gels (Bio-Rad, 456-8093), and separated by electrophoresis. Samples from the gels were transferred to nitrocellulose membranes (Bio-Rad, 170-4158) using the Trans-Blot system (Bio-Rad, 170-4155). Membranes were incubated for 1 h in a blocking solution on a plate shaker. The blocking solution contained 3 g of milk powder (Nestle, nonfat dry milk, Glendale, CA) dissolved in 100 ml of PBS-Tween. Tween was added to PBS (Bio-Rad, 170-6531, 1:1000 dilution) at the time of the experiment. Membranes were incubated with primary antibodies for Ezrin (Developmental Studies Hybridoma Bank, CPTC-Ezrin-1-s, 1:100 dilution with 0.5% milk in PBS-Tween), Moesin (Developmental Studies Hybridoma Bank, CPTC-MSN-1-s, 1:100 dilution with 0.5% milk in PBS-Tween), and myosin II (Developmental Studies Hybridoma Bank, CMII23, 1:500 dilution with 0.5% milk in PBS-Tween) for 10 min using the SNAP-id 2.0 system (SNAP2MB1, EMD Millipore). β-actin was used as the loading control (Sigma-Aldrich, A3854, dilution 1:5000), consistent with numerous previous cancer studies.[11,38,43–45] Membranes were washed 4 times in PBS-Tween solution for 5 min. Finally, the membranes were incubated with horseradish peroxidase-conjugated secondary antibody anti-mouse IgG (Jackson ImmunoResearch, 115035068, West Grove, PA) for 10 min with the SNAP-id system. Membranes were washed 4 times in fresh PBS-Tween solution for 5 min. The blots were revealed using the ECL (horseradish peroxidase substrate for enhanced chemiluminescence) solution (Bio-Rad, 170-5060) and visualized using an image analyzer system (ChemiDoc MP, 1708265, Bio-Rad). Expression levels were quantified using ImageJ software. Expression levels were normalized by β-actin loading control levels.

III. RESULTS

A. The number of blebbing prostate cells traversing a narrow microfluidic channel increases with metastatic potential

While performing power law cell rheology experiments with a microfluidic device at 37 °C (see Fig. 1), we observed that significantly more highly metastatic PC3 prostate cancer cells blebbed in the channel (56%) than moderately metastatic DU145 (38%, $p = 0.046$) or normal RWPE-1 prostate cells [29%, $p = 0.028$, Fig. 2(a)]. We also found that PC3 cells had a significantly higher average blebbing frequency (8.4 blebs/s) (defined as the number of blebs that form on a cell during its entry into the channel divided by the entry time) than DU145 (4.6 blebs/s, $p = 0.0045$) and RWPE-1 (3.5 blebs/s, $p = 0.0033$)—see Fig. 2(b). There were no significant differences in the average bleb diameter between the cell lines [Fig. 2(c), $p > 0.05$]. We observe that there is no overall trend between cell area and bleb occurrence while entering a narrow channel [Fig. 2(d)], i.e., no indication that the increased compression experienced by larger cells may push more fluid out of the cytosol, resulting in more blebs. PC3 cells have the largest area and more blebs per cell than DU145; however, RWPE-1 cells are not significantly larger than DU145 ($p > 0.05$) and have a significantly lower blebbing frequency ($p = 0.026$). Trypan blue was used in these experiments (see Sec. II) to identify and exclude nonviable cells in the recordings from analysis. The metastatic potential of

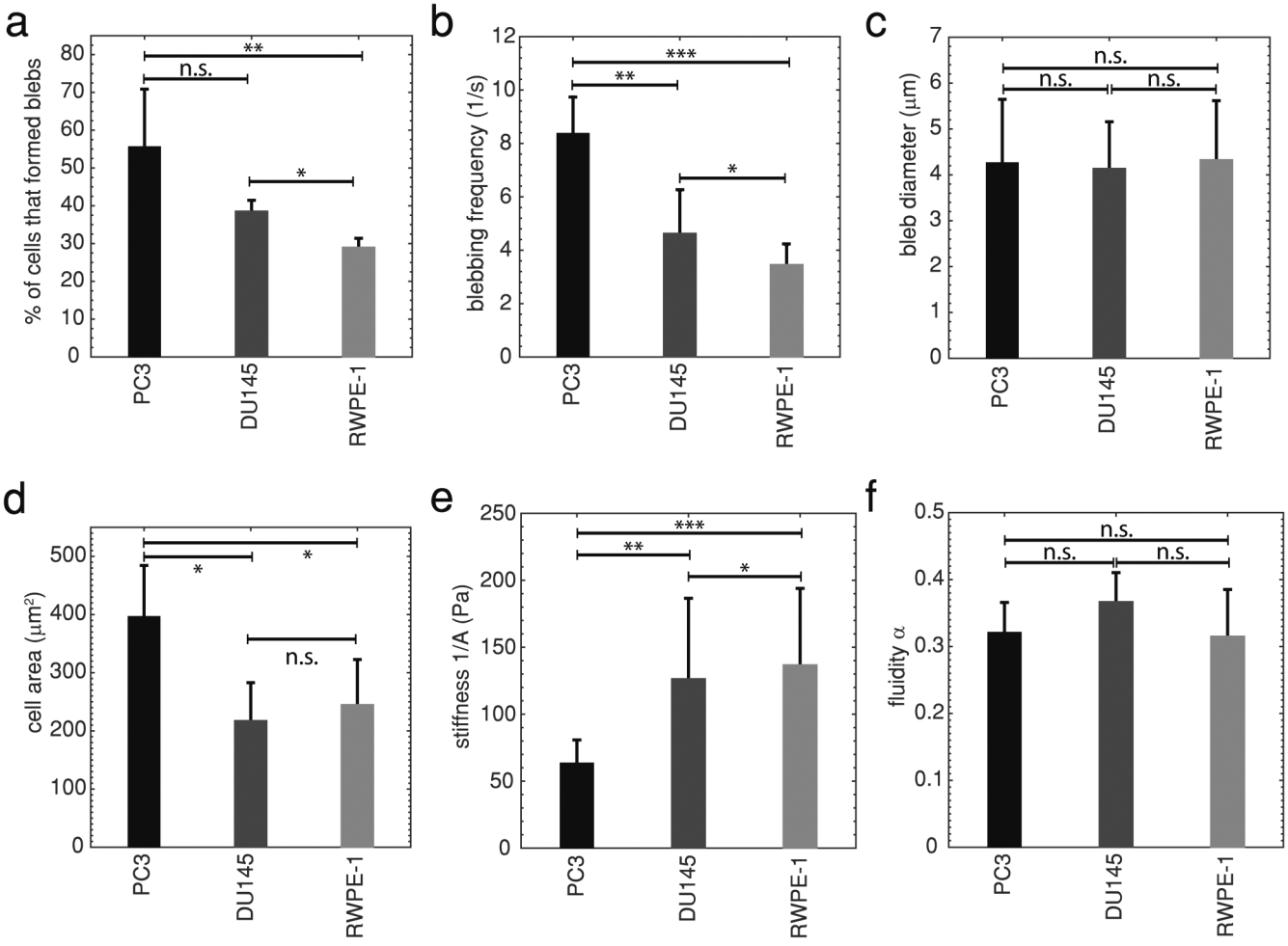

FIG. 2. (a) The average percentage of cells exhibiting blebbing ± SD in flow through a microfluidic channel. Highly metastatic PC3 n = 163, moderately metastatic DU145 n = 185, and normal RWPE-1 n = 241, *p = 0.046, **p = 0.028. (b) Average blebbing frequency, defined as the number of blebs formed on a cell while it is entering the channel divided by the entry time, ± SD. PC3 n = 35, DU145 n = 26, RWPE-1 n = 40, *p = 0.026, **p = 0.0045, ***p = 0.0033. (c) Average bleb diameter ± SD, n.s. indicates no statistical significance. (d) Average cell area ± SD, *$p \ll 1 \times 10^{-6}$. (e) Average cell stiffness ± SD, *p = 0.012, **p = 0.0078, ***$p \ll 1 \times 10^{-6}$. (f) Average cell fluidity ± SD. Statistical comparisons used one-way ANOVA followed by Tukey's *post hoc* test. Averages were taken from 3 or more independent experiments. For these experiments, the excess pressure drop $\Delta P = 1000$ Pa.

these cell lines was confirmed with wound scratch assays—highly metastatic PC3 cells migrate more quickly than moderately metastatic DU145 cells, and DU145 cells migrate more quickly than normal RWPE-1 cells—see Fig. 2 in the supplementary material. These findings indicate that the number of blebbing cells, and blebbing frequency, can be simple markers for highly metastatic prostate cancer.

1. Cell stiffness decreases with increasing metastatic potential

Metastatic cancer cells deform significantly while migrating to establish a new tumor site.[23] Due to this observation, it has been hypothesized and verified that some highly metastatic epithelial cancer cells are more deformable, or softer, than lowly metastatic or normal cells from the same organ.[17–22] Cell rheological parameters—stiffness $1/A$ and fluidity α—were measured for prostate cells entering a narrow microfluidic channel in a manner similar to micropipette aspiration (see Sec. II and Fig. 1),[38] much simpler to operate, to test this hypothesis. Both stiffness and fluidity were calculated from the cell rheological creep, where the stiffness quantifies a viscoelastic cell's resistance to deformation, and the fluidity describes the cell's flow like a viscous fluid or deformation like an elastic solid. All viscoelastic materials have $0 \leq \alpha \leq 1$, where 0 corresponds to an elastic solid and 1 to a viscous fluid. Figure 2(e) shows that normal RWPE-1 prostate cells are significantly stiffer than moderately metastatic DU145 ($p = 0.012$), and the latter are significantly stiffer than highly metastatic PC3 prostate cells ($p \ll 1 \times 10^{-6}$)—DU145 and RWPE-1 are more than twice as stiff as PC3. We also found that the fluidity of prostate cells ranged from 0.3 to 0.4 [Fig. 2(f)], consistent with previous micropipette cell aspiration studies.[40] These observations also support the use of stiffness as a marker for androgen insensitive metastatic prostate cancer.

B. Highly metastatic prostate cells bleb more under hypo-osmotic conditions

We next investigated whether highly metastatic cells bleb more than lowly metastatic and normal cells due to hypo-osmotic stress. It was previously found that stem cells bleb more in hypo-osmotic conditions than differentiated cells.[9] If highly metastatic cells bleb more, this method can be developed as an alternate PSA independent assay to identify metastatic prostate cancer cells. All cells were imaged for 12 h in control (normal osmolarity) and hypo-osmotic conditions (~ 50% osmolarity solution of ultrapure water and cell culture media—see Sec. II). Similar to our microfluidic bleb stimulation experiments, we found that under hypo-osmotic conditions significantly more highly metastatic PC3 cells had blebs (66%) than moderately metastatic DU145 (44%, $p = 0.0069$) and normal RWPE-1 cells (36%, $p = 0.02$)—see Fig. 3(b). Trypan blue was used to quantify cell viability after 12 h of treatment, which was not significantly different than control in all cases [$p > 0.05$, Fig. 3(c)]. While early-stage apoptosis cannot be identified with trypan blue, due to cells having intact plasma membranes at that stage, cells in late-stage apoptosis have permeable membranes that allow staining of the cells' intracellular proteins.[46] While cells bleb throughout the apoptotic process, early-stage blebbing typically lasts for 30–40 min after starting apoptosis, while late-stage blebbing often starts 60 min later.[47] Considering that at least 32% of all of the cells studied have blebbed after 12 h of hypo-osmotic treatment, this viability measurement rules out apoptotic cell blebbing—PC3 are 99.3% viable, DU145 are 98.3% viable, and RWPE-1 are 98.3% viable after 12 h of hypo-osmotic treatment. This suggests that blebbing due to hypo-osmotic conditions is also a potential metastatic cancer marker.

C. Highly metastatic cells have less F-actin and higher moesin levels, but similar ezrin and myosin II levels compared to moderately metastatic and normal cells

It has been suggested that the high incidence of blebbing in some cell types—including metastatic breast cancer and stem cells—is related to low expression of ERM (ezrin, radixin, and moesin) proteins that tether the plasma membrane to the actin cortex. Underexpression of these proteins can result in increased blebbing and has been associated with reduced stiffness of stem cells, breast cancer cells, and mesendoderm germ layer progenitor cells.[9,11,48] Figures 4(a)–4(b) show western blots and quantifications of ezrin and moesin proteins in highly metastatic PC3, moderately metastatic DU145, and normal RWPE-1 prostate cells. Blot quantifications show that differences in the ezrin levels among all cell lines are not significantly different ($p > 0.05$), and that highly metastatic PC3 cells express significantly more moesin than normal RWPE-1 prostate cells ($p = 0.013$). Our results indicate that increased blebbing of highly metastatic cells deforming in a microfluidic channel and reduced cell stiffness are not associated with reduced ERM protein expression.

Myosin II has been demonstrated to play a role in cell blebbing, as actomyosin contractions, generated by myosin II, increase cellular hydrostatic pressure leading to cortex rupture and bleb formation.[1–4] Western blots [Fig. 4(c)] show that prostate cells with different metastatic potential do not have significantly different myosin II levels ($p > 0.05$). Hypo-osmotic treatment also did not significantly change myosin II levels [Fig. 4(c)]. Therefore, in contrast with the literature,[1–4] myosin II expression does not strongly affect microfluidic and hypo-osmotic blebbing in prostate cells since the expression levels are not correlated with blebbing occurrence. Highly metastatic cancer cells frequently have decreased cortical F-actin, due to the cancer epithelial to mesenchymal transition (EMT),[49] which is known to induce a more migratory phenotype. We hypothesize that decreased F-actin leads to increased microfluidic and hypo-osmotic blebbing of highly metastatic prostate cells due to fewer ERM linker protein binding sites on the actin cortex. Studies have shown that decreasing F-actin with drug treatments increases Walker carcinosarcoma cell blebbing.[3,50] Supporting this hypothesis, an F-actin specific cell stain (Phalloidin), shown in Fig. 5(a), reveals that highly metastatic PC3 cells have less F-actin than moderately metastatic DU145 (75%, $p > 0.05$) and normal RWPE-1 prostate cells (69%, $p = 0.008$) [Fig. 5(b)]. Hypo-osmotic treatment does not significantly change F-actin fluorescence in highly metastatic prostate cells [$p > 0.05$, Fig. 5(b)] and significantly decreases F-actin fluorescence in lowly metastatic and normal cells ($p \ll 1 \times 10^{-6}$). It is also more difficult to distinguish cell boundaries for hypo-osmotic treatments due to the significantly reduced cortical actin—Fig. 5(a) also shows contrast enhanced and inverted contrast enhanced images. It is generally

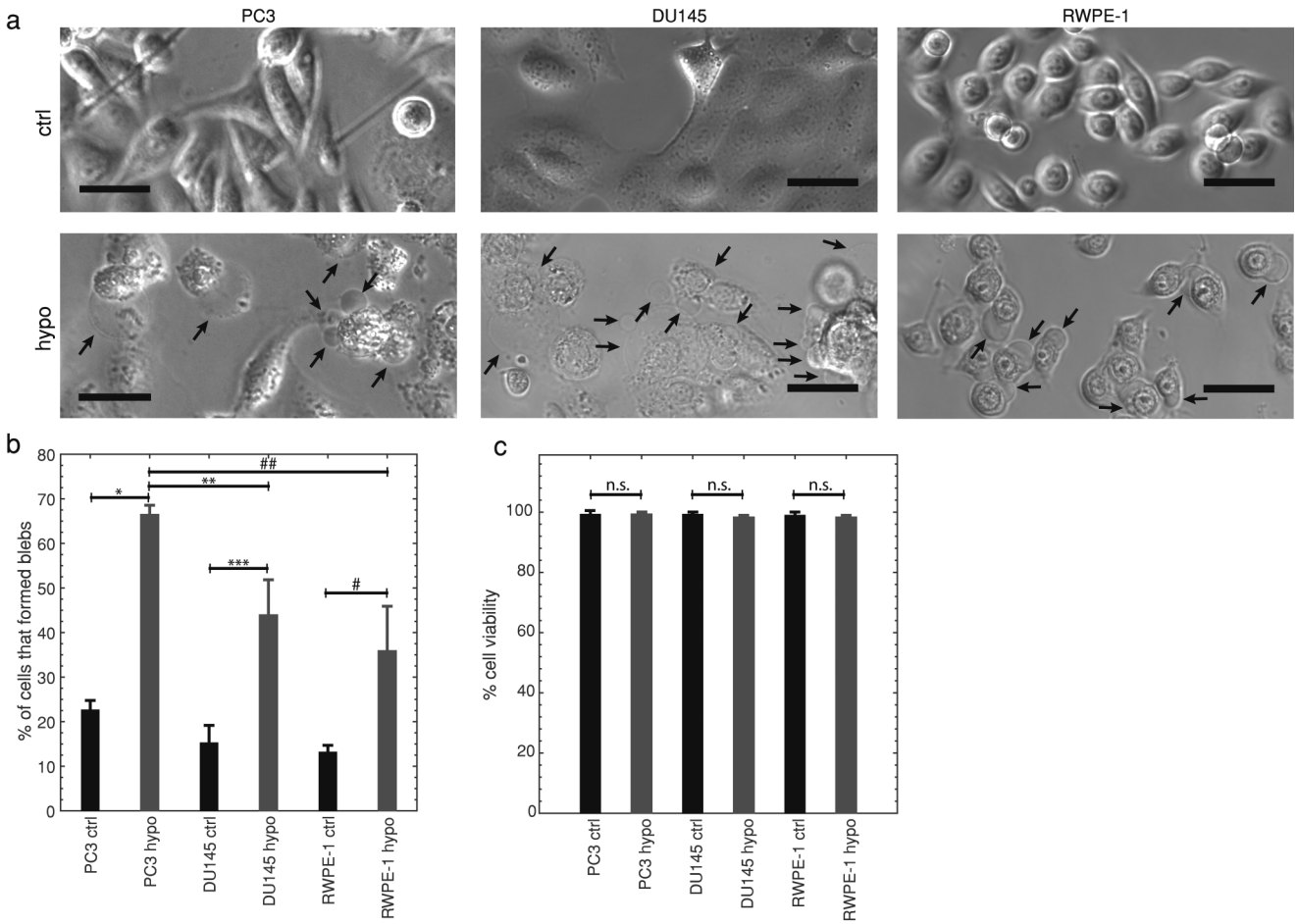

FIG. 3. (a) Representative bright-field images of highly metastatic PC3, moderately metastatic DU145, and normal RWPE-1 prostate cells in control iso-osmotic (ctrl) and hypo-osmotic (hypo) media for 12 h. Arrows indicate blebs, scale bars represent 40 μm. Images were linearly contrast enhanced by stretching gray scale values from the ranges [11, 199] (ctrl) and [0, 153] (hypo) to [0, 255] for PC3; [0, 130] (ctrl) and [22,210] (hypo) to [0,255] for DU145; and [0,163] (ctrl and hypo) to [0,255] for RWPE-1. Displayed images are cropped. (b) The average percentage of cells $\pm$ SD that formed blebs in hypo-osmotic media for 12 h in comparison with control, #p = 0.036, ##p = 0.02, *p = 0.0075, **p = 0.0069, ***p = 0.0052, one-way ANOVA followed by Tukey's *post hoc* test. Highly metastatic PC3 control n = 582, PC3 hypo-osmotic n = 527, moderately metastatic DU145 control n = 1169, DU145 hypo-osmotic n = 255, normal RWPE-1 control n = 507, RWPE-1 hypo-osmotic n = 494. (c) Average viability $\pm$ SD of hypo-osmotically treated (12 h) and control cells determined by Trypan blue stain exclusion. N.s. indicates no statistical significance, two-sample Kolmogorov–Smirnov test. Averages were obtained from 3 independent experiments.

accepted that cell swelling due to hypo-osmotic stress is accompanied by decreased F-actin expression,[51] and this decrease in F-actin may result in a cortex with fewer locations for ERM membrane connections. This likely contributes to blebbing, though further future study is warranted.

D. Metastatic cell blebbing while passing through a microfluidic channel does not vary with pressure drop, but stiffness and fluidity do

We performed microfluidic cell deformation experiments with different pressure drops acting across the cells at the channel entrance to test the robustness of microfluidic blebbing and cell stiffness as markers for metastatic potential since it is possible that higher pressure drops will promote increased ERM detachment. We found that the number of highly metastatic PC3 cells that bleb does not vary significantly with the pressure drop in the range of 1000–4000 Pa [Fig. 6(a), $p > 0.05$]. We also observed that normal RWPE-1 cells experienced the most significant increases in the number of blebbing cells at higher pressure drops—approximately 5% increases for each additional 1000 Pa of increased pressure ($p \leq 0.0032$). Since RWPE-1 cells express the lowest levels of moesin of the cell lines studied, this supports the possibility that higher pressure drops can promote ERM

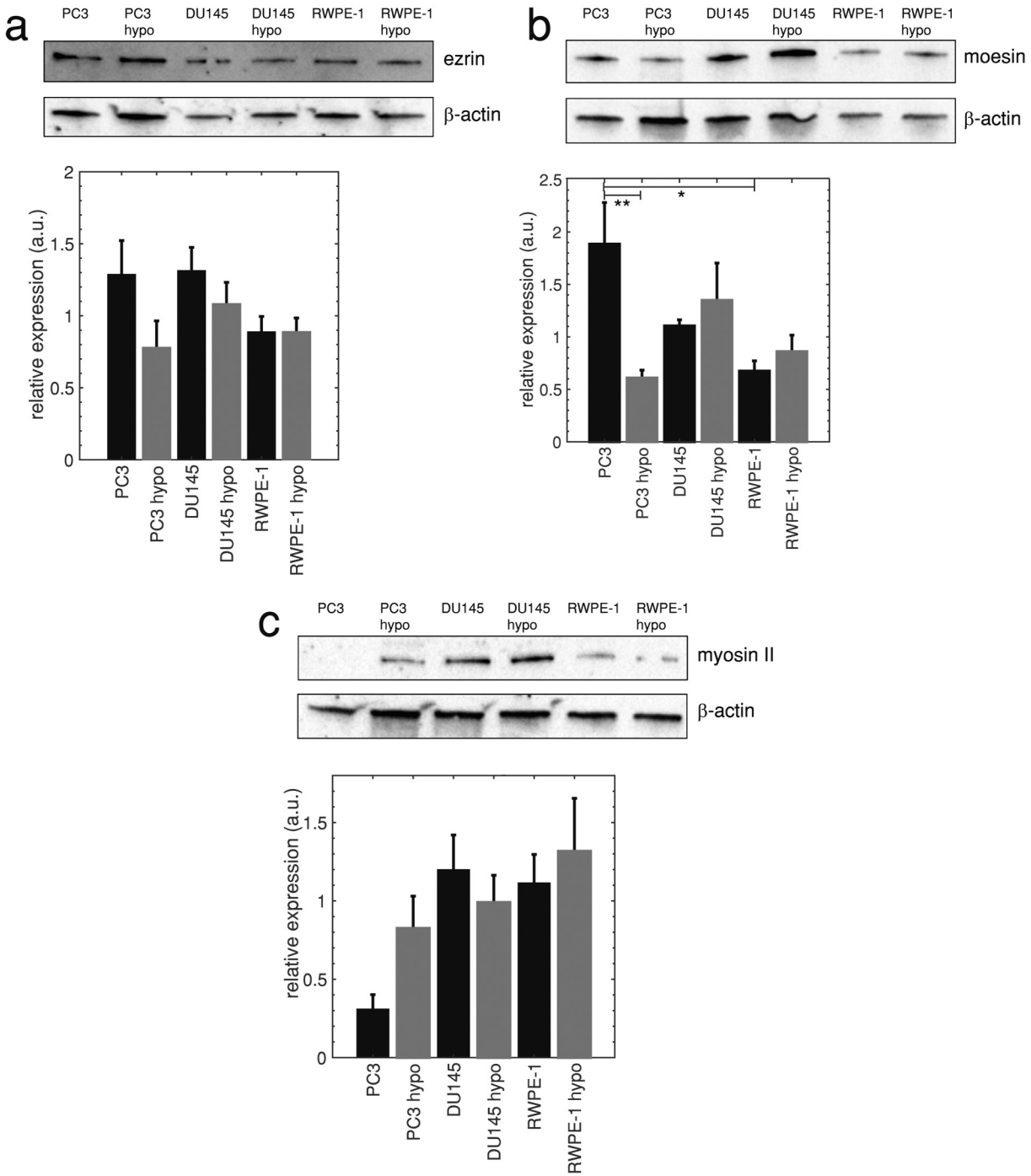

FIG. 4. (a) Ezrin levels in highly metastatic PC3, moderately metastatic DU145, and normal RWPE-1 prostate cells (upper panel), and average band densities normalized by β-actin loading control levels $\pm$ SEM (lower panel), n = 8, no statistical significance between prostate cell lines and hypo-osmotic conditions in comparison with control. (b) Moesin blots (upper panel) and average band densities normalized by β-actin $\pm$ SEM (lower panel), n = 5, *p = 0.013, **p = 0.0082. (c) Myosin II blots (upper panel) and average band densities normalized by β-actin loading control levels $\pm$ SEM (lower panel), n = 5, no statistical significance between prostate cell lines, and each cell line's hypo-osmotic conditions in comparison with control. Statistical comparisons used one-way ANOVA followed by Tukey's *post hoc* test. Cropped blots are displayed.

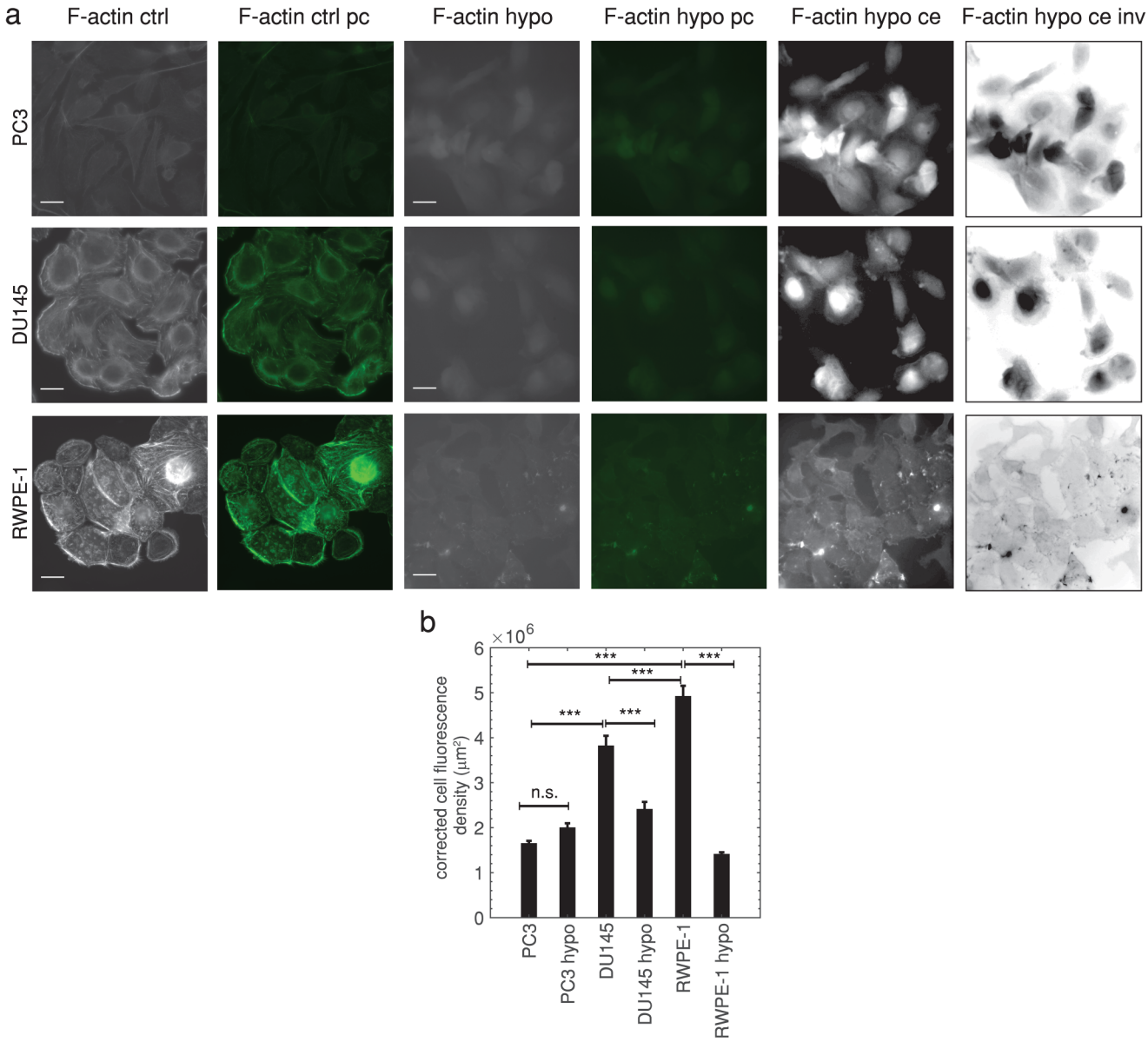

FIG. 5. (a) Fluorescence and green pseudocolor (pc) images of prostate cells labeled with F-actin specific Phalloidin-488 stain in iso-osmotic (ctrl) and hypo-osmotic (hypo) conditions. Scale bars represent 20 μm. Both linearly contrast enhanced (ce) and inverted linearly contrast enhanced mages (ce inv) are also shown for hypo conditions to enable visualization of cell boundaries. The following grayscale values were rescaled: [20, 120] to [0, 255] for PC3 hypo ce; [32, 50] to [0, 255] for DU145 hypo ce; [35, 81] to [0, 255] for RWPE-1 hypo ce. (b) Average corrected cell fluorescence density $\pm$ SEM for control (ctrl) and hypo-osmotic (hypo) conditions, n.s. = no significance ($p > 0.05$), ***$p \ll 1 \times 10^{-6}$, one-way ANOVA followed by Tukey's *post hoc* test. Additional comparisons were not statistically significant ($p > 0.05$). Highly metastatic PC3 control n = 332, PC3 hypo-osmotic n = 248, moderately metastatic DU145 control n = 240, DU145 hypo-osmotic n = 235, normal RWPE-1 prostate control n = 255, RWPE-1 hypo-osmotic n = 396. Averages were taken from 3 independent experiments.

plasma membrane and cortex linker detachment in some cell lines. It should be noted that the cancer cell lines still bleb $\sim$ 10% more than normal RWPE-1 cells at the highest pressure drop used (4000 Pa, the pressure drop where RWPE-1 cells bleb the most).

We additionally found that the cell fluidity decreases and stiffness increases significantly with an increased pressure drop ($p < 0.05$) for all cell types [Figs. 6(a)–6(c)]. This shows that the cells behave more solidlike, which can surprisingly lead to fewer cell deaths due to breakup under flow. This observation is

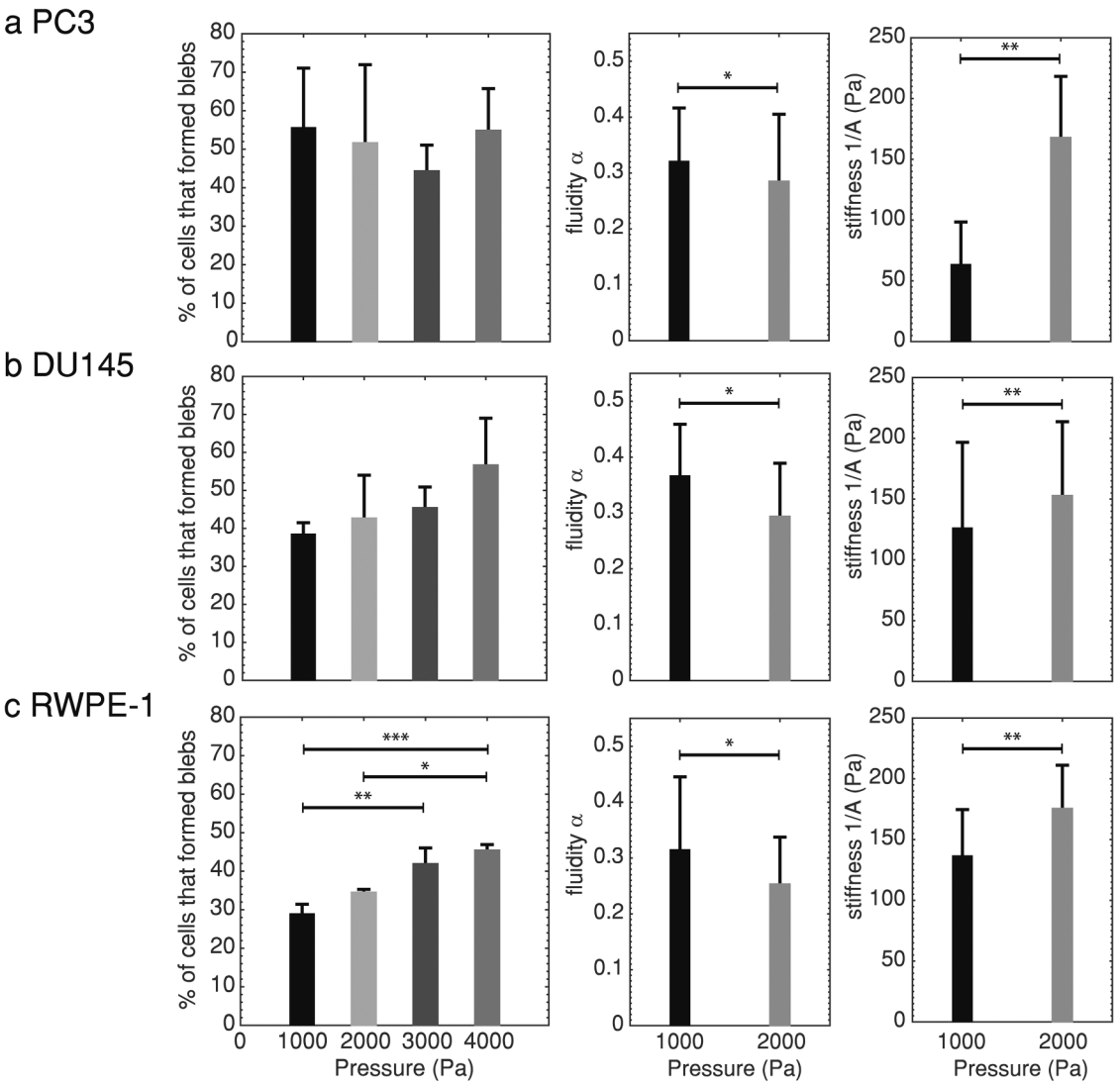

FIG. 6. (a) The average percentage of highly metastatic PC3 prostate cells that formed blebs ± SD (left, 1000 Pa: n = 167, 2000 Pa: n = 155, 3000 Pa: n = 213, 4000 Pa: n = 219, no statistical significance, one-way ANOVA), average cell fluidity ± SD (center, 1000 Pa: n = 35, 2000 Pa: n = 29, *p = 0.0065), and average cell stiffness ± SD (right, **$p \ll 1 \times 10^{-6}$). (b) The average percentage of moderately metastatic DU145 prostate cells that formed blebs ± SD (left, 1000 Pa: n = 185, 2000 Pa: n = 215, 3000 Pa: n = 221, 4000 Pa: n = 177, no statistical significance, one-way ANOVA), average fluidity ± SD (center, 1000 Pa: n = 26, 2000 Pa: n = 35, *p = 0.0019), and average stiffness ± SD (right, **p = 0.0075). (c) The average percentage of normal RWPE-1 prostate cells that formed blebs ± SD (left, 1000 Pa: n = 241, 2000 Pa: n = 245, 3000 Pa: n = 255, 4000 Pa: n = 303, *p = 0.0032, **p = 0.0011, ***p = 0.0002, one-way ANOVA followed by Tukey's *post hoc* test), average fluidity ± SD (center, 1000 Pa: n = 30, 2000 Pa: n = 16, *p = 0.047), and average stiffness ± SD (right, **p = 0.025). Averages were taken over 3 or more independent experiments. Each pressure drop used a new set of cells. Statistical comparisons between two groups used the two-sample Kolmogorov–Smirnov test.

consistent with several other rheological studies where cell stiffening was observed for increased applied stress.[52,53] *In vitro* shear deformation of prestressed cross-linked actin networks also exhibit stress stiffening.[54] Studies of fluidity changes with increased stress have yielded conflicting results; one such study observed a decrease in fluidity for increased optical stretching laser load,[55] while a magnetic tweezer study found that fluidity increased for increased applied force to cells.[53] A microfluidic cell rheology study reported that stiffness and fluidity are inherently connected; treatments that increase cell stiffness decrease fluidity.[56] Although nonlinear response of cellular creep to deformation has been implicated as a possible cause of these differing observations, the effect of stress on cell fluidity remains an unresolved issue and needs further study.

IV. DISCUSSION AND CONCLUSIONS

In this study, we have shown that highly metastatic prostate cancer cells are susceptible to membrane blebbing under stress using both microfluidic and hypo-osmotic conditions and that blebbing ability is reduced with decreased metastatic potential. We examined how cell mechanical properties influence blebbing and found, using the power law cell rheology model, that increased prostate cancer cell blebbing is correlated with low cell stiffness—in agreement with prior breast cancer and stem cell blebbing studies.[9,11] This suggests that both blebbing and cell stiffness can be biomechanical markers for metastatic androgen insensitive prostate cancer cells. The emphasis on blebbing in this paper is motivated by the prospect of using microfluidics to detect blebbing in a straightforward manner—much simpler than stiffness measurements, which can be used for simple and inexpensive clinical tools to detect highly metastatic prostate cancer cells that do not rely on PSA detection.

To examine the mechanism responsible for increased blebbing and reduced metastatic prostate cancer cell stiffness, we used western blots to measure differences in myosin II, ezrin, and moesin levels, and immunocytochemistry (ICC) to quantify actin levels. Myosin II has been linked to bleb formation by increasing cellular hydrostatic pressure—causing the membrane to detach from the cortex and fill with cytoplasmic fluid.[1–4] We found that highly metastatic cells express similar levels of myosin II as lowly metastatic and normal cells—indicating that myosin II likely does not play a key role in stress-induced blebbing. ERM membrane-cortex linker proteins are upregulated in some metastatic cancers;[57–59] however, their reduced expression has been correlated with increased blebbing in stem and breast cancer cells.[9–11] Our finding that highly metastatic prostate cancer cells express similar or higher levels of ezrin and moesin than moderately metastatic and normal cells suggests that these linker proteins do not suppress stress-induced prostate cancer cell blebbing. Increased ERM expression may actually stimulate blebbing, as these proteins can increase cortical tension[60] and increased cortical tension promotes blebbing.[2,59] Reduced ERM expression has also been previously correlated with reduced cell stiffness;[9,11,49] however, one study reports similar levels of ERM expression in stem and differentiated cells although the stem cells are nearly twice as stiff.[61] These suggest that the role of ERM expression alone in cell blebbing and stiffness is controversial and warrants further study.

We have shown that highly metastatic prostate cancer cells have less F-actin than moderately metastatic and normal cells—indicating that actin polymerization and organization have the strongest influence on prostate cancer cell blebbing and mechanics, consistent with one prior blebbing study.[62] Low F-actin may promote blebbing by providing fewer binding sites for ERM proteins to anchor the plasma membrane.[62] Many metastatic cancer cells express less cortical and cytoplasmic actin than normal cells[19,49]—this can result in the reduced cell stiffness observed for many cancer types including breast, lung, pancreatic, ovarian, melanoma, bladder, and colon cancers.[18,19,21,22] Reduced stiffness and increased deformability can give metastatic cells an advantage in navigating through small ECM and microvessel spaces.

Cancer cells are known to generate blebs (as opposed to lamellipodia) in response to both extracellular matrix protease inhibitor treatments, reduced substrate adhesiveness, and in 3D migration.[1] The observed plasticity in cancer cell migration modes results in more widespread metastasis as they can navigate effectively in differing environments.[7] Both blebability and stiffness may therefore be good markers for metastatic potential for other cancer types, in addition to androgen insensitive prostate cancer, as we have shown, for the first time.

We have also investigated changes in cellular mechanical properties and blebbing using a range of microfluidic pressure drops to test the robustness of our observations under different driving conditions and have found that differences in cell stiffness between cell lines are larger for lower pressure drops, while blebbing trends are not significantly affected. The ease in generating and observing blebs in suspended metastatic cells using microfluidic devices, as opposed to rheology measurements, indicates that the microfluidic method used here can be employed as an inexpensive and simple cancer diagnostic tool. Hypo-osmotic assays, also coupled with automated bleb detection and cell counting, can also be developed as an efficient high-throughput clinical tool for identifying metastatic adherent cells from biopsies.

SUPPLEMENTARY MATERIAL

See Fig. 1 in the supplementary material for microfluidic device schematic, and see Fig. 2 in the supplementary material for highly metastatic PC3, moderately metastatic DU145, and normal RWPE-1 prostate cell migration speeds.

ACKNOWLEDGMENTS

This study was funded by the President's Endowed Distinguished Chair in Engineering, Science, & Medicine funds (F.H.) and the Koh Family Engineering Scholarship (N.G.V.), Texas Tech University.

REFERENCES

[1]G. Charras and E. Paluch, "Blebs lead the way: How to migrate without lamellipodia," Nat. Rev. Mol. Cell Biol. **9**(9), 730–736 (2008).
[2]J.-Y. Tinevez, U. Schulze, G. Salbreux, J. Roensch, J.-F. Joanny, and E. Paluch, "Role of cortical tension in bleb growth," Proc. Natl. Acad. Sci. U.S.A. **106**(44), 18581–18586 (2009).
[3]M. Bergert, S. D. Chandradoss, R. A. Desai, and E. Paluch, "Cell mechanics control rapid transitions between blebs and lamellipodia during migration," Proc. Natl. Acad. Sci. U.S.A. **109**(36), 14434–14439 (2012).
[4]E. K. Paluch and E. Raz, "The role and regulation of blebs in cell migration," Curr. Opin. Cell Biol. **25**(5), 582–590 (2013).
[5]C. D. Paul, P. Mistriotis, and K. Konstantopoulos, "Cancer cell motility: Lessons from migration in confined spaces," Nat. Rev. Cancer **17**(2), 131 (2017).
[6]V. Te Boekhorst and P. Friedl, "Plasticity of cancer cell invasion—Mechanisms and implications for therapy," in *Advances in Cancer Research* (Elsevier, 2016), Vol. 132, pp. 209–264.
[7]P. Sekyrova, J. Östblom, and M. Andäng, "Blebbing as a physical force in cancer EMT—Parallels with mitosis," in *Seminars in Cancer Biology* (Elsevier, 2012), Vol. 22, pp. 369–373.
[8]A. Wells, J. Grahovac, S. Wheeler, B. Ma, and D. Lauffenburger, "Targeting tumor cell motility as a strategy against invasion and metastasis," Trends Pharmacol. Sci. **34**(5), 283–289 (2013).
[9]K. Sliogeryte, S. D. Thorpe, D. A. Lee, L. Botto, and M. M. Knight, "Stem cell differentiation increases membrane-actin adhesion regulating cell blebability, migration and mechanics," Sci. Rep. **4**, 7307 (2014).

[10]K. Sliogeryte, L. Botto, D. A. Lee, and M. M. Knight, "Chondrocyte dedifferentiation increases cell stiffness by strengthening membrane-actin adhesion," Osteoarthritis Cartilage **24**(5), 912–920 (2016).
[11]W. H. Lee, L. Y. Choong, N. N. Mon, S. Lu, Q. Lin, B. Pang, B. Yan, V. Sri Ram Krishna, H. Singh, and T. Z. Tan, "TRPV4 regulates breast cancer cell extravasation, stiffness and actin cortex," Sci. Rep. **6**, 27903 (2016).
[12]S. Tai, Y. Sun, J. M. Squires, H. Zhang, W. K. Oh, C.-Z. Liang, and J. Huang, "PC3 is a cell line characteristic of prostatic small cell carcinoma," Prostate **71** (15), 1668–1679 (2011).
[13]E. C. Faria, N. Ma, E. Gazi, P. Gardner, M. Brown, N. W. Clarke, and R. D. Snook, "Measurement of elastic properties of prostate cancer cells using AFM," Analyst **133**, 1498–1500 (2008).
[14]J. Concato, C. K. Wells, R. I. Horwitz, D. Penson, G. Fincke, D. R. Berlowitz, G. Froehlich, D. Blake, M. A. Vickers, G. A. Gehr *et al.*,"The effectiveness of screening for prostate cancer: A nested case-control study," Arch. Intern. Med. **166**(1), 38–43 (2006).
[15]B. J. Feldman and D. Feldman, "The development of androgen-independent prostate cancer," Nat. Rev. Cancer **1**(1), 34–45 (2001).
[16]D. Yamazaki, S. Kurisu, and T. Takenawa, "Regulation of cancer cell motility through actin reorganization," Cancer Sci. **96**(7), 379–386 (2005).
[17]J. Rother, H. Nöding, I. Mey, and A. Janshoff, "Atomic force microscopy-based microrheology reveals significant differences in the viscoelastic response between malign and benign cell lines," Open Biol. **4**(5), 140046 (2014).
[18]K. Hayashi and M. Iwata, "Stiffness of cancer cells measured with an AFM indentation method," J. Mech. Behav. Biomed. Mater. **49**, 105–111 (2015).
[19]A. Calzado-Martín, M. Encinar, J. Tamayo, M. Calleja, and A. San Paulo, "Effect of actin organization on the stiffness of living breast cancer cells revealed by peak-force modulation atomic force microscopy," ACS Nano **10**(3), 3365–3374 (2016).
[20]J. Guck, "Feeling for cell function-mechanical phenotyping at 1,000 cells/sec," Biophys. J. **110**(3), 342a (2016).
[21]K. D. Nyberg, S. L. Bruce, A. V. Nguyen, C. K. Chan, N. K. Gill, T.-H. Kim, E. K. Sloan, and A. C. Rowat, "Predicting cancer cell invasion by single-cell physical phenotyping," Integr. Biol. **10**(4), 218–231 (2018).
[22]S. Byun, S. Son, D. Amodei, N. Cermak, J. Shaw, J. H. Kang, V. C. Hecht, M. M. Winslow, T. Jacks, P. Mallick, and S. R. Manalis, "Characterizing deformability and surface friction of cancer cells," Proc. Natl. Acad. Sci. U.S.A. **110**, 7580–7585 (2013).
[23]J. M. Northcott, I. S. Dean, J. K. Mouw, and V. M. Weaver, "Feeling stress: The mechanics of cancer progression and aggression," Front. Cell Dev. Biol. **6**, 17 (2018).
[24]L. Bastatas, D. Martinez-Marin, J. Matthews, J. Hashem, Y. J. Lee, S. Sennoune, S. Filleur, R. Martinez-Zaguilan, and S. Park, "AFM nano-mechanics and calcium dynamics of prostate cancer cells with distinct metastatic potential," Biochim. Biophys. Acta **1820**, 1111–1120 (2012).
[25]R. G. Bedolla, Y. Wang, A. Asuncion, K. Chamie, S. Siddiqui, M. M. Mudryj, T. J. Prihoda, J. Siddiqui, A. M. Chinnaiyan, and R. Mehra, "Nuclear versus cytoplasmic localization of filamin A in prostate cancer: Immunohistochemical correlation with metastases," Clin. Cancer Res. **15**(3), 788–796 (2009).
[26]C. J. Loy, K. S. Sim, and E. L. Yong, "Filamin-A fragment localizes to the nucleus to regulate androgen receptor and coactivator functions," Proc. Natl. Acad. Sci. U.S.A. **100**(8), 4562–4567 (2003).
[27]K.-P. Janssen, L. Eichinger, P. A. Janmey, A. A. Noegel, M. Schliwa, W. Witke, and M. Schleicher, "Viscoelastic properties of f-actin solutions in the presence of normal and mutated actin-binding proteins," Arch. Biochem. Biophys. **325**(2), 183–189 (1996).
[28]W. H. Goldmann, M. Tempel, I. Sprenger, G. Isenberg, and R. M. Ezzell, "Viscoelasticity of actin-gelsolin networks in the presence of filamin," FEBS J. **246**(2), 373–379 (1997).
[29]K. Wolf, S. Alexander, V. Schacht, L. M. Coussens, U. H. von Andrian, J. van Rheenen, E. Deryugina, and P. Friedl, "Collagen-based cell migration models *in vitro* and *in vivo*," Sem. Cell Dev. Biol. **20**, 931–941 (2009).
[30]S. E. Lee, R. J. Jin, S. G. Lee, S. J. Yoon, M. S. Park, D. S. Heo, and H. W. Choi, "Development of a new plasmid vector with PSA-promoter and enhancer expressing tissue-specificity in prostate carcinoma cell lines," Anticancer Res. **20**(1A), 417–422 (2000).
[31]D. Bello, M. M. Webber, H. K. Kleinman, D. D. Wartinger, and J. S. Rhim, "Androgen responsive adult human prostatic epithelial cell lines immortalized by human papillomavirus 18," Carcinogenesis **18**(6), 1215–1223 (1997).
[32]Yu. M. Efremov, A. A. Dokrunova, A. V. Efremenko, M. P. Kirpichnikov, K. V. Shaitan, and O. S. Sokolova, "Distinct impact of targeted actin cytoskeleton reorganization on mechanical properties of normal and malignant cells," Biochim. Biophys. Acta **1853**(11), 3117–3125 (2015).
[33]R. Alert, J. Casademunt, J. Brugués, and P. Sens, "Model for probing membrane-cortex adhesion by micropipette aspiration and fluctuation spectroscopy," Biophys. J. **108**(8), 1878–1886 (2015).
[34]B. Maugis, J. Brugués, P. Nassoy, N. Guillen, P. Sens, and F. Amblard, "Dynamic instability of the intracellular pressure drives bleb-based motility," J. Cell Sci. **123**(22), 3884–3892 (2010).
[35]A. Chlenski, K.-I. Nakashiro, K. V. Ketels, G. I. Korovaitseva, and R. Oyasu, "Androgen receptor expression in androgen-independent prostate cancer cell lines," Prostate **47**(1), 66–75 (2001).
[36]Y. Mirochnik, D. Veliceasa, L. Williams, K. Maxwell, A. Yemelyanov, I. Budunova, and O. V. Volpert, "Androgen receptor drives cellular senescence," PLoS One **7**(3), e31052 (2012).
[37]Y. Xia and G. M. Whitesides, "Soft lithography," Annu. Rev. Mater. Sci. **28**, 153–184 (1998).
[38]J. M. Santos, Z. S. Khan, M. T. Munir, K. Tarafdar, S. M. Rahman, and F. Hussain, "Vitamin d_3 decreases glycolysis and invasiveness, and increases cellular stiffness in breast cancer cells," J. Nutr. Biochem. **53**, 111–120 (2017).
[39]Z. S. Khan, N. Kamyabi, F. Hussain, and S. A. Vanapalli, "Passage times and friction due to flow of confined cancer cells, drops, and deformable particles in a microfluidic channel," Convergent Sci. Phys. Oncol. **3**(2), 024001 (2017).
[40]E. H. Zhou, S. T. Quek, and C. T. Lim, "Power-law rheology analysis of cells undergoing micropipette aspiration," Biomech. Model Mechanobiol. **9**, 563–572 (2010).
[41]D. P. Theret, M. J. Levesque, M. Sato, R. M. Nerem, and L. T. Wheeler, "The application of a homogeneous half-space model in the analysis of endothelial cell micropipette measurements," J. Biomech. Eng. **110**, 190–199 (1988).
[42]A. Burgess, S. Vigneron, E. Brioudes, J.-C. Labbé, T. Lorca, and A. Castro, "Loss of human greatwall results in G2 arrest and multiple mitotic defects due to deregulation of the cyclin B-Cdc2/PP2A balance," Proc. Natl. Acad. Sci. U.S.A. **107**(28), 12564–12569 (2010).
[43]S. Bhattacharyya, S. Saha, K. Giri, I. R. Lanza, K. Sreekumar Nair, N. B. Jennings, C. Rodriguez-Aguayo, G. Lopez-Berestein, E. Basal, A. L. Weaver *et al.*, "Cystathionine beta-synthase (CBS) contributes to advanced ovarian cancer progression and drug resistance," PLoS One **8**(11), e79167 (2013).
[44]S. A. Melo, H. Sugimoto, J. T. O'Connell, N. Kato, A. Villanueva, A. Vidal, L. Qiu, E. Vitkin, L. T. Perelman, and C. A. Melo, "Cancer exosomes perform cell-independent microRNA biogenesis and promote tumorigenesis," Cancer Cell **26**(5), 707–721 (2014).
[45]S. Fernandez, M. Risolino, N. Mandia, F. Talotta, Y. Soini, M. Incoronato, G. Condorelli, S. Banfi, and P. Verde, "miR-340 inhibits tumor cell proliferation and induces apoptosis by targeting multiple negative regulators of p27 in non-small cell lung cancer," Oncogene **34**(25), 3240 (2015).
[46]A. K. Jain, D. Singh, K. Dubey, R. Maurya, S. Mittal, and A. K. Pandey, "Models and methods for *in vitro* toxicity," in *In Vitro Toxicology* (Academic Press, 2018), pp. 45–65.
[47]J. D. Lane, V. J. Allan, and P. G. Woodman, "Active relocation of chromatin and endoplasmic reticulum into blebs in late apoptotic cells," J. Cell Sci. **118**(17), 4059–4071 (2005).
[48]A. Diz-Muñoz, M. Krieg, M. Bergert, I. Ibarlucea-Benitez, D. J. Muller, E. Paluch, and C.-P. Heisenberg, "Control of directed cell migration *in vivo* by membrane-to-cortex attachment," PLoS Biol. **8**(11), e1000544 (2010).

[49]J. Shankar and I. R. Nabi, "Actin cytoskeleton regulation of epithelial mesenchymal transition in metastatic cancer cells," PLoS One **10**(3), e0119954 (2015).
[50]H. Keller, P. Rentsch, and J. Hagmann, "Differences in cortical actin structure and dynamics document that different types of blebs are formed by distinct mechanisms," Exp. Cell Res. **277**(2), 161–172 (2002).
[51]S. F. Pedersen, E. K. Hoffmann, and J. W. Mills, "The cytoskeleton and cell volume regulation," Comparative Biochem. Physiol. Part A Mol. Integr. Physiol. **130**(3), 385–399 (2001).
[52]D. Icard-Arcizet, O. Cardoso, A. Richert, and S. Hénon, "Cell stiffening in response to external stress is correlated to actin recruitment," Biophys. J. **94**(7), 2906–2913 (2008).
[53]P. Kollmannsberger, C. T. Mierke, and B. Fabry, "Nonlinear viscoelasticity of adherent cells is controlled by cytoskeletal tension," Soft Matter **7**(7), 3127–3132 (2011).
[54]M. L. Gardel, F. Nakamura, J. H. Hartwig, J. C. Crocker, T. P. Stossel, and D. A. Weitz, "Prestressed f-actin networks cross-linked by hinged filamins replicate mechanical properties of cells," Proc. Natl. Acad. Sci. U.S.A. **103**(6), 1762–1767 (2006).
[55]J. M. Maloney, E. Lehnhardt, A. F. Long, and K. J. Van Vliet, "Mechanical fluidity of fully suspended biological cells," Biophys. J. **105**(8), 1767–1777 (2013).
[56]J. R. Lange, J. Steinwachs, T. Kolb, L. A. Lautscham, I. Harder, G. Whyte, and B. Fabry, "Microconstriction arrays for high-throughput quantitative measurements of cell mechanical properties," Biophys. J. **109**, 26–34 (2015).
[57]J. Clucas and F. Valderrama, "ERM proteins in cancer progression," J. Cell Sci. **127**(2), 267–275 (2014).
[58]G. A. Ponuwei, "A glimpse of the ERM proteins," J. Biomed. Sci. **23**(1), 35 (2016).
[59]L. S. Hinojosa, M. Holst, C. Baarlink, and R. Grosse, "MRTF transcription and ezrin-dependent plasma membrane blebbing are required for entotic invasion," J. Cell Biol. **216**(10), 3087–3095 (2017).
[60]P. Kunda, A. E. Pelling, T. Liu, and B. Baum, "Moesin controls cortical rigidity, cell rounding, and spindle morphogenesis during mitosis," Curr. Biol. **18**(2), 91–101 (2008).
[61]I. Titushkin and M. Cho, "Regulation of cell cytoskeleton and membrane mechanics by electric field: Role of linker proteins," Biophys. J. **96**(2), 717–728 (2009).
[62]Z. Wang, A. K. T. Wann, C. L. Thompson, A. Hassen, W. Wang, and M. M. Knight, "IFT88 influences chondrocyte actin organization and biomechanics," Osteoarthritis Cartilage **24**(3), 544–554 (2016).